Synthesis, Characterization and Sorptive Removal of Heavy metals on Nano-Structured Agglomerates of Iron (III)-Cerium (IV) Bimetal Mixed Oxide (NICMO): Search For An Efficient, Low Cost Decontamination Technique

Tina De[1*], Abir Ghosh[1], Uday Chand Ghosh[1]
[1]Department of Chemistry, Presidency University, 86/1 College Street, Kolkata-700073

Abstract

Nano particles usually exhibit remarkable physical properties, rapid chemical reactivity, and high sorption capacity for inorganic compounds. Studies of the fate and transport of nano particles were largely concerned with their properties and behavioral change over time, whether they would interact with toxic contaminants after being released into the environment.Keeping in line with the above facts, here, we aim to develop an efficient material by eco-friendly green synthetic route that was further characterized to be crystalline ranging in nano-dimension for filtering heavy metals containing groundwater. The average particle size was found to be approximately 3.56 nm calculated from the Gaussian fit of the distinct peaks and then computing its modeled data into Scherrer's equation.The thermal stability of iron(III)-cerium(IV) mixed oxide nanoparticle agglomerates (NICMO) was well established from the consistent particle size at different temperature and also, from differential thermal. The bimetal mixed oxide contained agglomerated crystalline nano-particles of dimension 10-20 nm held together by crystal packing forces and, its corresponding empirical composition $FeCe_{1.1}O_{7.6}$. Appearance of weak band at 534 cm^{-1} in the FTIR spectrum of NICMO is presumed for the presence of hetero- metal bonding via oxygen linkage (i.e, Fe-O-Ce). Scanning electron microscopic (SEM) image of NICMO established the agglomerated surface morphology with irregular shape that was unevenly dispersed over a base matrix of oxide surface almost covering up its porous nature. Decreasing sharpness of inflexion points of NICMO in BET isotherm indicates porosity arising out of channels of the template framework but surely with non uniformity in pore size distribution.The positive change in entropy ($\Delta S°$) values of both Pb(II) and Cd(II) species with NICMO in the systems investigated conclude that the reactions were entropy driven, occurring with increase of randomness at solid-liquid interface owing to the release of water molecules when hydrated Pb(II) and Cd(II) species binds on to the solid surface

Keywords Nano-dimension,surface morphology, pore size distribution, solid-liquid interface

Introduction

The multifold increase in the use of heavy metals over the past few decades has inevitably resulted in an increased flux of metallic substances into the environment. Water pollution has become an emergent anxiety over the last century as more and more waste is being disposed off in water bodies. The presence of metal ions in industrial waste water, ground water and soils can pose a significant threat to human health and ecological systems.

Heavy metal ions in water pose a serious threat to human health and environment due to their toxic effects, carcinogenicity, bio- accumulation and non- biodegradability **[1]**. Heavy metals such as lead (Pb), cadmium (Cd), arsenic (As), mercury (Hg), and chromium (Cr) are the most concerned as these are potentially accountable for most of the heavy metal related diseases. Heavy metal ions such as Cd(II) and Pb(II) are dangerously toxic to the public health for their high mobilization ability via complex formation through surface soil onto the groundwater. Cd(II) & Pb(II) have been known as carcinogens. The Water Supply (Water

Corresponding author
Email address: tina.de@iemcal.com

Quality) Regulations 2000 of United Kingdom suggested that the maximum allowed concentration (MAC) limit is 0.005 ppm in drinking water for cadmium. On the other hand EPA drinking water standards for lead are 0.02 ppm. Lead has no significant use and biological function in human body, but its presence has severe impact on health of children as well as adults which include harsh toxic effect such as damage of brain, cancer, hepatitis, nerve disorders, high blood pressure, renal failure, anaemia, insomnia, reproductive problems [2]. The key sources of lead are mainly industrial processes such as lead smelting, battery manufacturing, ceramic and glass manufacturing industries, printing and pigment, iron and steel manufacturing [3].

Cadmium is considered as a non-essential and a highly toxic element possibly because it forms a strong bond with sulphur and hence, can displace essential metals e.g, Zn^{2+} and Ca^{2+} from the binding sites of certain enzymes. Cadmium is extensively used in manufacturing Ni–Cd cells, metal plating, metallurgical alloying, fertilizers, mining, etc. Chronic exposure in Cd(II) is known to cause lung insufficiency, bone lesions, kidney damage and hypertension in mammals and humans.

To avoid health problems due to intake of excess metal ions, several methods developed for the treatment of contaminated water are surface adsorption, chemical precipitation, ion-exchange, nano-filtration, membrane separation, reverse osmosis, etc. Among them, surface adsorption is found to be the most popular method for easy operation, reusability, the requirement of less space and cost effectiveness. Adsorption of Cd(II) for the removal was investigated using sugar beet pulp [4], iron ore slime [5], macro fungus biomass [6], algal biomass [7] etc.

On the other hand, adsorption of Pb(II) for the removal was also investigated using various adsorbents such as activated carbon, iron oxides, filamentous fungal biomass, natural condensed tannin etc have been explored [8].

Despite the materials tested are cheap yet their low removal capacities limit their usability in practice. Adsorption capacity and reusability of ion- exchange resins are a quite satisfactory but low thermal stability and high production cost limit the practical utility in third world countries like India.

Ceria nano-particles were considered to be a representative member of an industrially important class of metal oxide nano-particles; they could be used as automotive catalytic converters**, UV-blocking agents**, and single, nanowire- based gas sensors**. Owing to the presence of high affinity surface hydroxyl groups, hydrous cerium oxide (HCO) nano-partices showed encouraging sorption capacity. Therefore, we have aimed to investigate the sorption behavior of Pb(II) and Cd(II) on nano-structured iron(III)-cerium(III) mixed oxide (NICMO) and report systematically.

Materials and Methods

Chemicals
The stock solutions (1000 mg·L^{-1}) of Cd(II) and Pb(II) were made separately by dissolving an appropriate amount of cadmium(II) chloride and Lead(II) nitrate, (guaranteed reagents, E. Merck India) in slightly acidic solution (1.5% nitric acid) that were further diluted to get the desired concentrations for the experiments. The exact concentration of each test solution was analyzed by atomic absorption spectrophotometer (AAS) against the standard.

Synthesis of NICMO
Solutions of ferric chloride (0.1M) and ACN (0.1M) were prepared separately by dissolving appropriate amounts in 0.1 M hydrochloric acid. Then, ACN solution was added slowly to

ferric chloride solution with vigorous stirring (v/v = 1:1). To it 5(M) sodium hydroxide solution was added drop wise into the above mixture with continuous stirring to increase pH 9.0 to 9.5.The gel like precipitate with mother liquid was allowed to stand for 48 hours before filtration without disturbing. The filtered precipitate was washed three times with distilled water and dried at 100°C in an air oven. The dried product was ground in a mortar and pestle and sieved to separate the agglomerates having dimension ranged in 140-290 μm. The sieved material was homogenized at pH 7.0 (± 0.2) before its use in experiments.

Results and Discussions

Physicochemical characterization of NICMO
XRD pattern analysis

X-ray diffraction (XRD) patterns of (a) iron(III) oxide, (b) cerium(IV) oxide and (c) NICMO samples have been shown in **Fig. 1A**, which showed crystalline nature of the samples. Comparison of °2θ values for the XRD peak positions of three synthetic materials have shown that the two peaks were identical with CeO_2 phase having cubic structures corresponding to (hkl) values (111) and (220), and one common to Ce_2O_3 phase having hexagonal structures corresponding to the (hkl) value (201), respectively. However, only one XRD peak of NICMO has been found close to α-Fe_2O_3, indicating incorporation of some Fe^{3+} ion in to the crystal structure of cerium oxide either by replacement or occupying void space. It has also revealed that the sharpness of XRD peaks of CeO_2 (pattern-b, Fig. 1A) is greater than that of NICMO owing to the incorporation of Fe^{3+} ions into the well defined crystallites of CeO_2. The broader peaks of XRD patterns of NICMO than its corresponding pure counterparts (CeO_2 or Fe_2O_3) was presumably due to the crystal strain owing to the substitution of some Ce^{4+} (0.97 Å) by smaller Fe^{3+} (0.65 Å) in the unit cell.
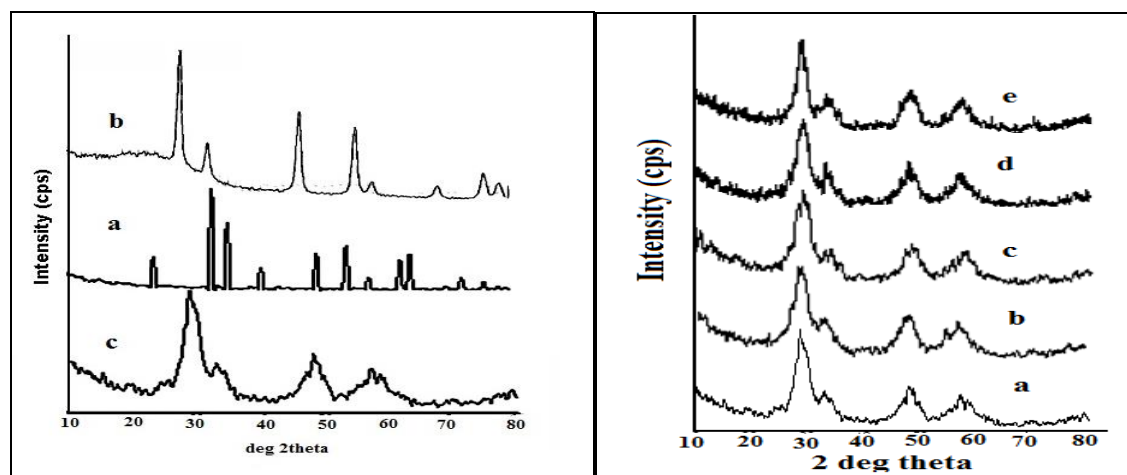
Figure 1A: X-ray diffraction patterns of synthetic (a) Fe_2O_3, (b) CeO_2 and (c) NICMO

Figure 1B: X-ray diffraction patterns of NICMO calcined at (°C) (a) 100, (b) 200, (c) 300, (d) 400, (e) 500

XRD patterns of the NICMO samples prepared by calcining at 100°, 200°, 300°, 400° and 500° C temperatures respectively have been shown in **Fig. 1B**. Comparing the peaks at °2θ values (= 28.5°, 33.1°, 47.5°, 56.6° and 58.28°) among the calcined samples with the standard JCPDS data has established (**Table-1a)** that the peak at °2θ = 33.1 was common to all calcined NICMO samples, indicating α-Fe_2O_3 phase of hematite variety having rhombohedra structures with (h k l) value (104). The peaks obtained at °2θ = 28.5° (hkl = 111) and 47.5° (hkl = 220) are for the cubic CeO_2 in NICMO.

The well-defined XRD peak at °2θ = 56.6° obtained for NICMO sample calcined at 100˚C has been assigned for the hexagonal Ce_2O_3 phase (hkl = 201). The lowering of intensity of this peak and gradual superimposing with the adjacent peak with increasing incinerated

temperature from 200°C might be due to the oxidation of Ce(III) to Ce(IV) at higher temperature. The XRD peak that appeared at $°2\theta = 58.28°$ was presumably due to the formation of some mixed phase in the sample prepared by initial heating at 100°C, that has become more prominent with increasing calcined temperatures. Thus, the well-defined Ce_2O_3 phase of NICMO (dried at~70°C) has almost disappeared owing to its conversion to thermodynamically more favored CeO_2 phase with increment of calcination temperature on that material.

Table-1(a): Comparison of x-ray diffraction data of NICMO with relevant JCPDS International Centre for Diffraction data.

	Comparison of peak of NICMO with CeO_2						Comparison of peak of NICMO with α-Fe_2O_3					
Incineration temperature (°C)	2θ (exp)	2θ (JCPD)	Intensity	H	K	l	Incineration temperature (°C)	$°2\theta$ (exp)	$°2\theta$ (JCPD)	Intensity	h	k	l
100	28.5	28.54	999	1	1	1	100	33.1	33.18	999	1	0	4
100	47.49	47.48	458	2	2	0							

The size of NICMO particles as-calculated from the Gaussian fit of the distinct peaks and computing its modeled data into the Scherrer's equation has been found to be 3.6 1±0.17) nm (Table-1b**)** for the samples prepared by calcination at 100°, 200°, 300°, 400° and 500° C temperatures respectively.

Analysis of the XRD patterns of NICMO samples prepared by incinerating at temperature (C) 100°, 200°, 300°, 400° and 500° suggested that the sample material did neither segregate nor aggregate with increasing temperature indicating reasonable thermal stability.

Table-1(b): Variation of average particle size (nm) of incinerated NICMO

Incineration temperature (°C) of NICMO	Average particle size (nm)
100	3.65
200	3.78
300	3.45
400	3.68
500	3.50

The nature of the XRD pattern and its concurrent particle size data have been found to be consistent at different incinerated temperatures emphasizing the thermal stability of the synthesized NICMO.

The weight loss (24.32 %) at temperature range < 90° C arises from the loss of water as found in TG analysis, which has been confirmed from the sharp endothermic band obtained at temperature ranged in 60°-90°C in DT spectrum. The thermal stability of the sample at higher temperature agreed well with the XRD patterns obtained at higher temperature.

Fourier transform infra-red spectroscopy (FTIR)

Föurier transform infra red (FTIR) spectra for iron (III) oxide (spectrum-a), cerium (IV) oxide (spectrum-b) and NICMO (spectrum-c) have been demonstrated in supporting information (Fig. 4).

Bands (spectra- a to c, Fig. S1) that appeared at wave number (υ, cm^{-1}) range 3700-3300 and 1750-1600 are due to the symmetrical and asymmetrical stretching and bending vibration modes of O-H bonds of hydroxyl groups, respectively. Additionally, the absorption band around 870 cm^{-1} in pure iron (III) oxide (spectrum-a) and 860 cm^{-1} in pure cerium (IV) oxide (spectrum-b) are probably for the metal- oxygen (Fe-O and Ce-O) bonds, respectively. Bands at wave number (cm^{-1}) 1385 and 1060 cm^{-1} are presumed for symmetrical and asymmetrical bending vibration of metal bonded hydroxyl group (M-OH) in the bimetal mixed oxide, respectively (spectrum-c). Appearance of a weak band at 534 cm^{-1} in the spectrum-c of NICMO **(Fig. 4)** is presumed for the hetero metal oxygen bond (Fe-O-Ce). Thus, the oxide as-prepared by the precipitation method has been characterized as a bimetal hydrous mixed oxide.
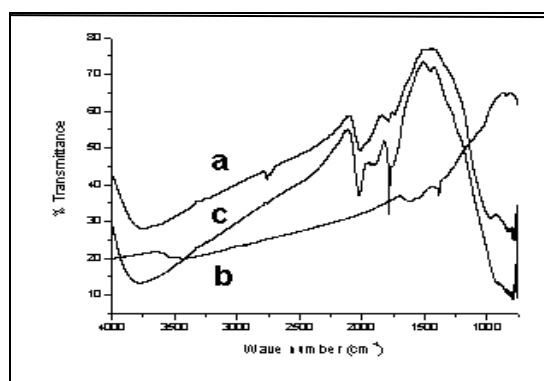
Figure- 4: FTIR analysis of (a) Synthetic Iron(III) oxide, (b) Synthetic Cerium(IV) oxide, and (c) Iron(III)-Cerium (IV) bimetal mixed oxide formed by chemical precipitation (NICMO)

Scanning electron microscopic (SEM) image of NICMO

Fig. 5(a) shows SEM image of NICMO, which established the agglomerated surface morphology with irregular shape that was unevenly dispersed over a base matrix of oxide surface almost covering up its porous nature. SEM image of NICMO with EDAX analyzed data at marked site [(Fig. 5(b)] shows that the surface mean percentage (parenthesis) composition of NICMO sample was O (37.39), Ce (47.52) and Fe (17.06), indicating Fe: Ce mole ratio to 1: 1.1 and empirical composition $FeCe_{1.1} O_{7.6}$.
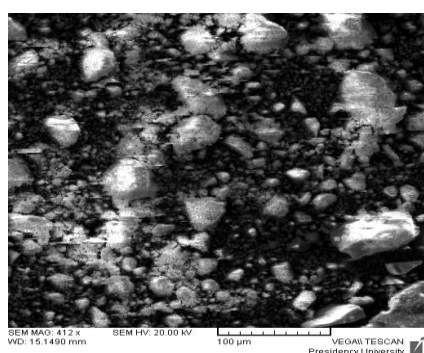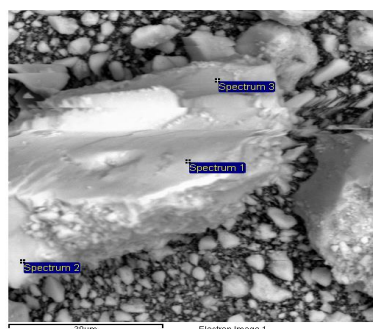
(a)   (b)

Figure5. .Scanning electron microscopic (SEM) image of (a) NICMO (b) Scanning electron microscopic (SEM) image with EDAX data of NICMO

Figure5. .Scanning electron microscopic (SEM) image of (a) NICMO (b) Scanning electron microscopic (SEM) image with EDAX data of NICMO

Transmission electron microscopic (TEM) image of NICMO Transmission electron microscopic (TEM) image of NICMO with 4.3×10^4 fold magnification has been shown in Fig. 6.

Spectrum	In stats.	O	Fe	Ce	Total
Spectrum 1	Yes	40.47	13.91	45.62	100.00
Spectrum 2	Yes	7.29	17.85	74.85	100.00
Spectrum 3	Yes	34.31	16.27	49.42	100.00
Mean		27.36	16.01	56.63	100.00
Std. deviation		17.65	1.98	15.90	
Max.		40.47	17.85	74.85	
Min.		7.29	13.91	45.62	

All results in weight%

The size of crystallite particles ranged between 8 to 10 nm under crystal packing force as estimated from the TEM image. The crystallites size of NICMO obtained by inserting XRD peak data into Scherrer's equation (3.56 nm) were found to be lower than that obtained from the TEM image owing to the approximation incorporated to drive that solid state physics equation. Microcrystalline nature with crystallite size 8 to 10 nm packed within NICMO agglomerates under crystal packing forces is estimated from TEM image analysis which is about 2.5 times greater compared to XRD data.
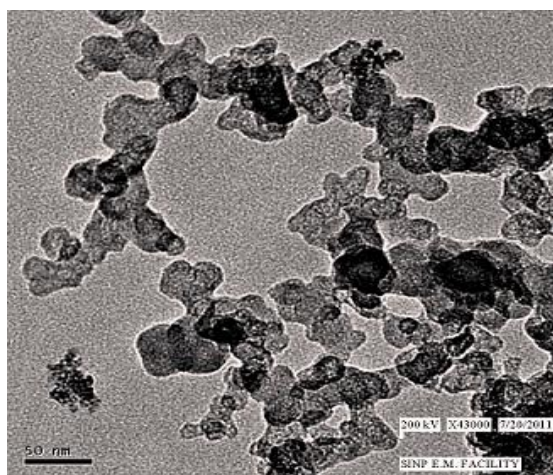
Figure6.Transmission electron microscopic image of NICMO

BET surface area analysis of NICMO

Plots of (A) $N_{2(vapor)}$ adsorption-desorption and (B) pore size distribution of NICMO has been presented in **Fig. 7**. The isotherm clearly showed the gradual increase of adsorption from P/P_o 0.1 to 0.2 followed by a large and two small inflections at P/P_o ranged in 0.1 to 0.35, 0.55 to

0.65 and 0.65 to 0.75. The hysteresis loop (Fig. 4A) in N_2 isotherm indicated the framework porosity of NICMO that ranged between 0.4-0.7 P/P_o within the uniform channels of the templated framework, while the textural porosity at 0.8-1.0 P/P_o had arisen from the non-crystalline intra-aggregate voids and spaces formed by inter-particle contacts [9, 10]. Thus, careful examination revealed that the porosity has arisen out of channels of the template framework but surely with non uniformity in pore size distribution as evidenced from decreasing sharpness of inflexion points. The latter isotherm was associated with an irregular desorption hysteresis. The BET surface area of NICMO had been obtained as 104 $m^2. g^{-1}$, which was lower than the specific surface area of cerium(IV) oxide (122 $m^2. g^{-1}$) but higher than iron(III) oxide (98 $m^2. g^{-1}$). The surface area ($m^2. g^{-1}$) of the material is 104 as obtained from the BET isotherm analysis, which is lower than pure Ce(IV) oxide (122) and higher than Fe(III) oxide (98). Higher pore volume (0.132 $cm^3.g^{-1}$) estimated from $N_{2(V)}$ adsorption-desorption isotherm predicts good adsorbent possibility of the material.

Results indicated (**Fig. 7**) that the pore volume of the sample was 0.132 $cm^3. g^{-1}$. The narrow pore size distribution of NICMO (shown in Fig. 7B) had suggested that the sample has a maximum pore size 5.68 nm.

(a)   (b)
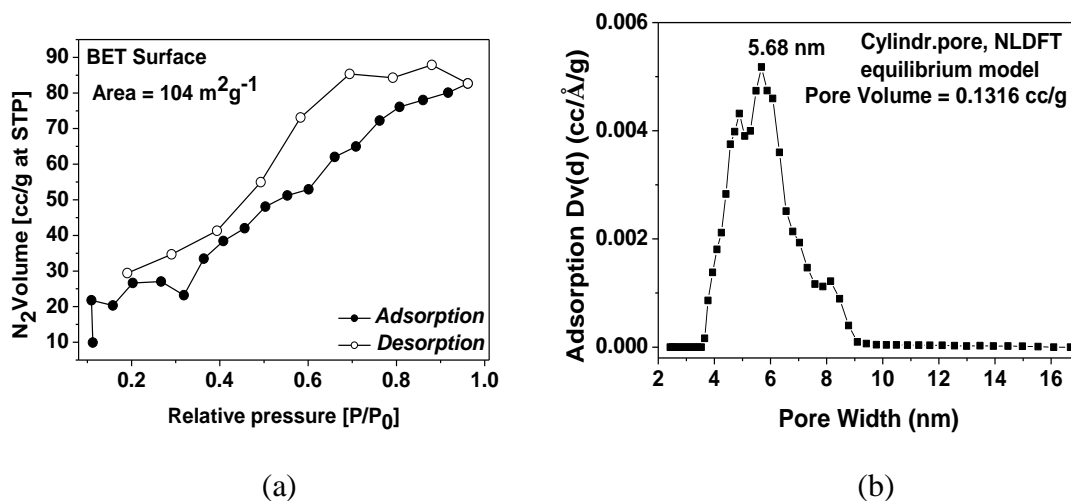
Figure7.(a) N_2 adsorption-desorption plot. (b)Pore size distribution plot of NICMO

Raman Effect

Fig.8 exhibited Raman spectrum of NICMO. No characteristic peaks of either synthetic iron(III) oxide or cerium(IV) oxide had been observed in this spectrum indicating the bimetal mixed oxide was not just a physical mixture of the two. In addition, sharp peaks were observed within the range 2000-2300 cm^{-1}which might be due to the presence of hetero-metal bonding via oxygen linkage (Fe-O-Ce). Peaks at ~ 3500 cm^{-1} are owing to the presence of surface hydroxyl (O-H) groups on the oxide surface.
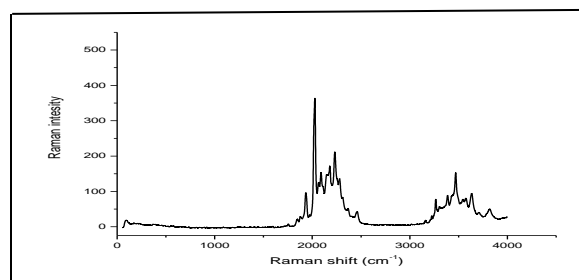
Figure- 8: Raman spectra of cerium(IV) associated iron(III) bimetal mixed oxide sorbent (NICMO)

The analyzed physical characteristics of NICMO sample were summarized in Table-2

Table-2: Summarized physical characteristic features of NICMO sample

Physical Characteristic Parameters of NICMO	Physical Characteristics
Average particle size (XRD Analysis) (nm)	3.56
Band Assignment in FTIR Spectra (cm^{-1})	Hetero-metal bridging at 534.
pH$_{ZPC}$	7.13 ($\pm$ 0.1)
Empirical formula derived from SEM Analysis	FeCe$_{1.1}$ O$_{7.6}$
Particle size (TEM) Analysis) (nm)	10 to 20
BET Surface Area (m^2. g^{-1})	104

Effect of pH

Fig. 9 (a, b & c) demonstrates the sorption capacity of Cd(II) and Pb(II) from their aqueous solutions of concentration 5.0 and 10.0 mg. L^{-1} respectively against initial solution pH (pH$_i$) from 2.0 to 9.0 . It was found that the metal ion sorption capacity increases rapidly with increasing pH$_i$ from 0 to 5.0, and there after it remain almost constant or slowly decreased. Further which it was followed by steady increase at higher pH (pH $\geq$ 8.0). Comparison of the data with control experiments showed that removal of Cd(II) and Pb(II) before pH$_i$ 6.0 by other principles were insignificant because the OH$^-$ concentration before pH 6.0 is insufficient to overcome the solubility product of M(OH)$_2$ where M=Cd(II)/Pb(II). However, removal of Cd(II) or Pb(II) increased at higher pH owing to precipitation, because the OH$^-$ concentration after pH 8.0 is sufficient to overcome the solubility product of M(OH)$_2$ .Thus, the pH$_i$ was optimized to be 5.0 for removal of the metal ions from their aqueous solutions.
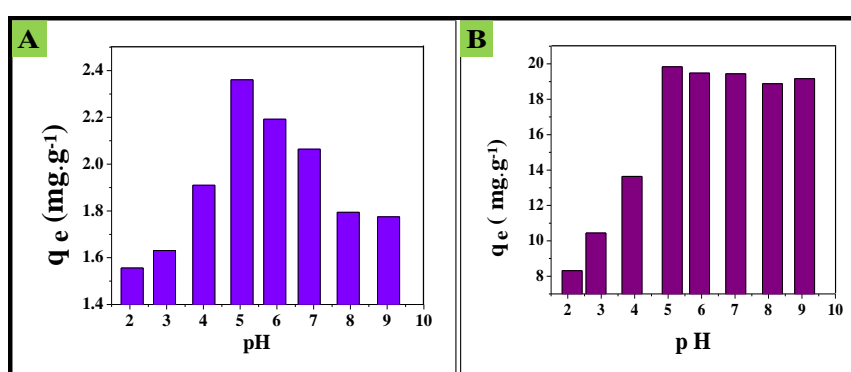
Figure- 9: Effect of initial solution pH on (A) Cd (II) and (B) Pb (II) sorption

Kinetic modeling
For the analysis of kinetic data the two kinetic equations viz. pseudo first order and pseudo-second order equation were used .The non-linear form of the equations are given below in

Table-3k_1 (min^{-1}) and k_2 (mg. g^{-1}. min^{-1}) are rate constants, q_e (mg. g^{-1}) the equilibrium sorption capacity, and q_t (mg. g^{-1}) is the amount of adsorption at time, t (min).

Figure 10 demonstrates q_t (mg. g^{-1}) versus reaction time (t, min) at T = 303 ± 1.6 K and pH$_i$ = 5.0 ± 0.2 on NICMO. It was observed that q_t increased rapidly in the first 50 minutes where more than 80-85% of the sorption occurred in case of Cd(II) sorption **(Fig. 10 A and B)**. While 90% of Pb(II) sorption was almost completed within 35-40 minutes while remaining 10-15% sorption took place between 50 and 120 mins as shown in **(Fig. 10 C and D)**. Results showed that the time required to reach equilibrium increased with increasing adsorbate concentration. The parameters calculated from the analysis of modeled kinetic equation had been given in **Table 3(a, b)** for Cd(II) and Pb(II) respectively.

Table-3(a): Kinetic parameters estimated for Cd(II) sorption onto NICMO at 30°C and pH$_i$ = 5.0 (±0.2)

Kinetic models	Kinetic parameters	Concentration(mg. dm^{-3})	
		5.0	**10.0**
Pseudo-first order	χ^2	0.0113	0.17
	R^2	0.7086	0.8641
	k_1(min.$^{-1}$)	0.0856	0.0311
	q_e (mg.g^{-1})	0.9497	3.9323
Pseudo-second order	χ^2	0.004	0.097
	R^2	0.8959	0.9225
	k_2 (mg. g^{-1}min^{-1})	0.0129	0.0084
	q_e (mg.g^{-1})	1.0334	4.5893

Table- 3(b): The kinetic parameters estimated for Pb(II) sorption onto NICMO at 30°C and pH$_i$ = 5.0 (±0.2)

Kinetic models	Kinetic parameters	Concentration(mg. dm^{-3})	
		5.0	**10.0**
Pseudo-first order	χ^2	0.0113	0.0473
	R^2	0.7086	0.8039
	k_1(min.$^{-1}$)	0.0856	0.1541
	q_e (mg.g^{-1})	0.9496	3.1213
Pseudo-second order	χ^2	0.004	0.0065
	R^2	0.8959	0.9729
	k_2 (mg.g^{-1}min^{-1})	0.1293	0.0722
	q_e (mg.g^{-1})	1.0333	3.3407

Analysis of the result showed that pseudo-second order kinetic model fit was better than that of first in case of sorption reaction of both the metals onto NICMO surface. Pseudo-second order rate constant values (k_2) decreased with increase of initial metal ion concentration for both the sorption reactions. This was due to higher time required to reach equilibrium for higher concentration of metal ion (10.0 mg/l).
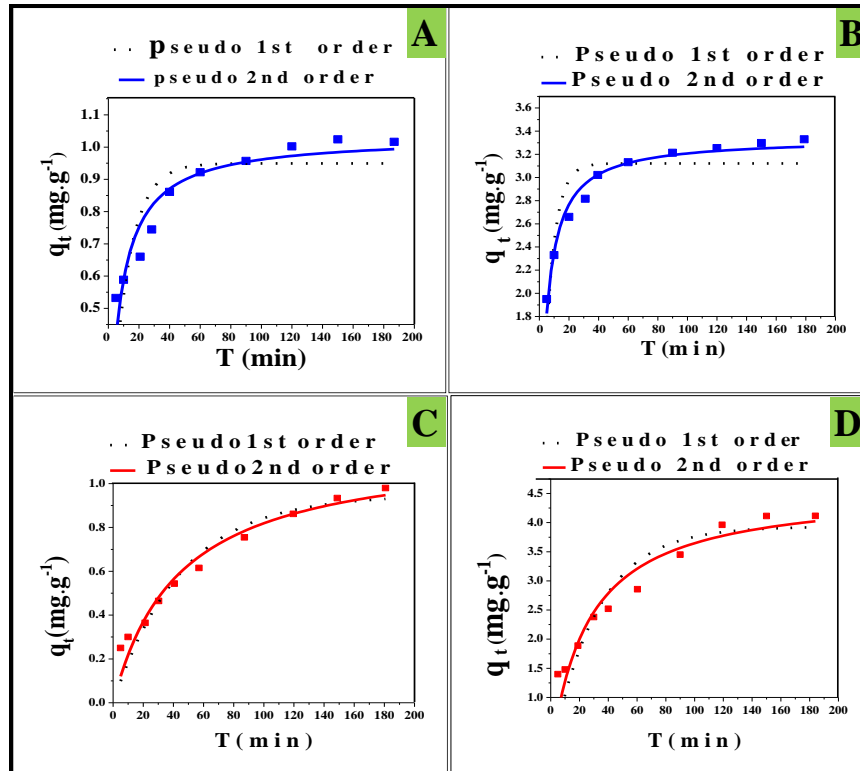
Figure 10: Kinetic modeling of Pb, Cd sorption on NICMO
(A) 5 ppm (B) 10 ppm Pb solution, (C) 5 ppm (D) 10 ppm Cd solution

Isotherm modeling

For the analysis of equilibrium data, two isotherm equations viz Langmuir (27) and Freundlich (28) were used. The detailed of the equations has been given in **table-II** where q_e is the equilibrium sorption capacity (mg.g^{-1}), C_e the equilibrium concentration (mg. dm^{-3}), q_m, the Langmuir monolayer adsorption capacity (mg. g^{-1}) and b is the binding constant (dm^3. mg^{-1}) for the sites of identical energy, K_F (mL$^{1/n}$ mg$^{1-1/n}$) and n (dimensionless) are the Freundlich constants.

Variations of q_e (mg·g^{-1}) against Ce (mg· L^{-1}) were demonstrated in Figs. 11 (A, B & C) and 11(D, E & F), respectively, for Cd(II) and Pb(II) sorption reaction at temperature 15°, 30°and 45 °C. The data for Cd(II) and Pb(II) sorptions by NICMO were separately analyzed by isotherm models using non-linear regression fit method. It was found that the equilibrium data described the Langmuir model better than Freundlich model for both the metal ions. Values of Langmuir monolayer sorption capacity q_m (mg/g) increased with increasing reaction temperature. This indicated that the availability of higher energy sorption sites of the adsorbents increased with increasing temperature of the reactions. Langmuir monolayer sorption capacity q_m (mg/g) were 3.16, 8.84 and 10.99 while that of 7.40, 11.01 and 17.18 respectively for Cd(II) and Pb(II) sorption reaction onto NICMO surface at temperature 15, 30 and 45 °C. This indicated that the available higher energy active site consequently increases with increase of temperature since greater amount of adsorbate was sorbed at the

sorbent surface. This also indicated the endothermic nature of Cd(II) sorption onto NICMO surface. Identical trends of observations were also found in case of Pb(II) sorption reaction

Table- 4(a): The isotherm parameters estimated for Cd(II) sorption onto NICMO at different temperatures and pH$_i$ = 5.0 ($\pm$0.2)

Isotherm models	Isotherm parameters	Temperature (ºC)		
		15	30	45
Langmuir	χ^2	2.405	0.0798	0.1006
	R^2	0.9640	0.9482	0.9865
	b (dm^3. mg^{-1})	0.5603	0.0496	0.2686
	q$_m$ (mg.g^{-1})	3.16441	8.8409	10.9912
Freundlich	χ^2	0.01457	0.1132	0.5404
	R^2	0.97822	0.9266	0.9278
	n	3.25554	1.2689	2.3050
	K$_F$	1.29582	0.4733	2.4099

Table- 4(b): The isotherm parameters estimated for Pb(II) sorption onto NICMO at different temperatures and at pH$_i$ = 5.0 ($\pm$0.2)

Isotherm models	Isotherm parameters	Temperature (º C)		
		15	30	45
Langmuir	χ^2	0.16921	0.24155	0.19082
	R^2	0.96661	0.97931	0.98549
	b (dm^3. mg^{-1})	1.09265	1.42379	0.45849
	q$_m$ (mg.g^{-1})	7.42969	11.01408	17.17869
Freundlich	χ^2	.34474	0.67835	.62933
	R^2	0.93198	0.94188	0.95214
	n	3.06012	2.74684	2.27015
	K$_F$	3.70218	5.87384	5.77023
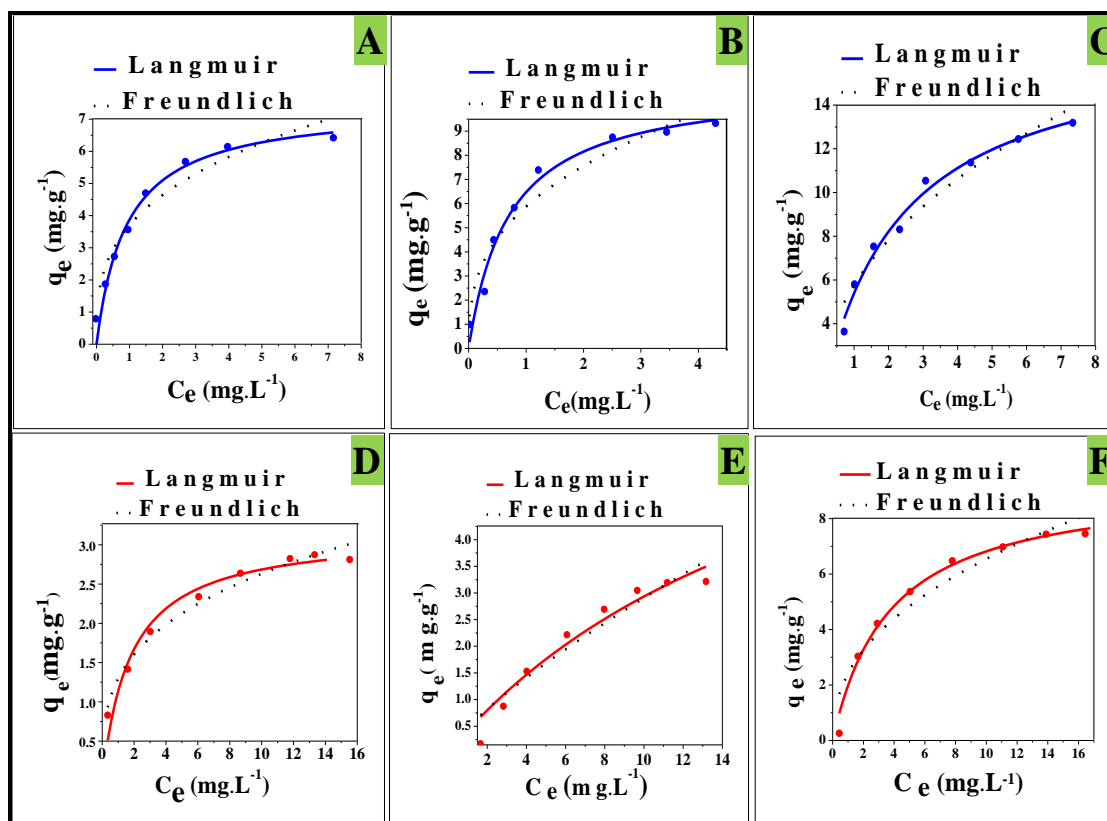
Figure 11: Isotherm modeling of sorption of Pb (K) at (A) 288, (B) 303, (C) 313 and Cd (K) at (D) 288 (E) 303 (F) 313 on NICMO

Conclusion

Present work explore a new cheaper and selective sorbent (NICMO) as an alternative of costly sorbents for the separation of Pb(II) and Cd(II) ions. The main advantages of procedure are the ease and simplicity of preparation of sorbent, sensitivity, rapid attainment of phase equilibration and high capacity values. Sorption of Cd(II) and Pb(II) on NICMO obeyed pseudo-second order kinetics and Langmuir sorption isotherm. The monolayer sorption capacity increase with increasing temperature on the reactions.

References

[1]   J. Chawla, R. Kumar, I. Kaur, Carbon nanotubes and graphenes as adsorbents for adsorption of lead ions from water: a review, J. of Water Supply: Research and Technology AQUA, 64 (6) (2015) 641–659

[2]   O. Yavuz, R. Guzel, F. Aydin, I. Tegin, R. Ziyadanogullari, Removal of cadmium and lead from aqueous solution by calcite. Polish Journal of Environmental Studies, 16 (3) (2007) 467–471.

[3]   S. K. Srivastava, V. K. Gupta, D. Mohan, Removal of lead and chromium by activate slab– A blast furnance waste, Journal of Environmental Engineering, 123 (1999) 461–468.

[4]   Y.N. Mata, M.L. Blázquez, A. Ballester, F. González, J.A. Muñoz, Sugar beet pulp pectin gels as biosorbent for heavy metals: preparation and determination of biosorption and desorption characteristics, Chem. Eng. J. 150 (2009) 289–301.

[5]   M. Mohapatra, K. Rout, B. K. Mohapatra, S. Anand, Sorption behaviour of Pb(II) and Cd(II) on iron ore slime and characterization of metal ion loaded sorbent, J. Hazard. Mater. 166 (2009) 1506–1513

[6]   R. A. Anayurt, A. Sari, M. Tuzen, Equilibrium, thermodynamic and kinetic studies on biosorption of Pb(II) and Cd(II) from aqueous solution by macrofungus (Lactarius scrobiculatus) biomass, Chem. Eng. J. 151 (2009) 255–261

[7] V.J.P. Vilar, S.C. Santos, R.J.E. Martins, C.M.S. Botelho, R.A.R. Boaventura, Cadmium uptake by algal biomass in batch and continuous (CSTR and packed bed column) adsorbers, Biochem. Eng. J. 42 (2008) 276–289.

[8] Y.H. Li, Z.C. Di, J. Ding, D.H.Wu, Z.K. Luan, Y.Q. Zhu, Adsorption thermodynamic, kinetic and desorption studies of Pb2+ on carbon nanotubes, Water Res. 39 (2005) 605–609.

[9] Zhang, Y., Yang, M., Don, X.M. Arsenate adsorption on an Fe-Ce bimetal oxide adsorbent: role of surface properties. Environ. Sci. Technol. **39** (2005) 7246-7253.

[10] Kim, Y., Kim, C., Choi, I., Rengaraj, S., Yi, J. Arsenic Removal Using Mesoporous Alumina Prepared via a Templating Method. Environ. Sci. Technol. **38** (2004) 924-931.